Nanoparticle-Mediated Local and Remote Manipulation of Protein Aggregation

Marcelo J. Kogan,*,[†,‡] Neus G. Bastus,[§] Roger Amigo,[§] Dolors Grillo-Bosch,[†,||]
Eyleen Araya,[‡] Antonio Turiel,[⊥] Amilcar Labarta,[§] Ernest Giralt,[†,||] and
Victor F. Puntes*,[#]

*Institut de Recerca Biomèdica de Barcelona, Parc Científic de Barcelona-UB, Josep
Samitier 1-5, 08028 Barcelona, Spain, Departamento de Farmacología y Toxicología,
Facultad de Ciencias Químicas, Universidad de Chile. Olivos 1007, Santiago, Chile,
Departament de Física Fonamental, Universitat de Barcelona, 647 Av Diagonal,
08028 Barcelona, Spain, Departament de Química Orgànica, Universitat de
Barcelona, Martí i Franquès, 1-11, 08028 Barcelona, Spain, Centre Mediterrani
d'Investigacions Marines i Ambientals, CMIMA-CSIC, Passeig Marítim de la
Barceloneta, 37-49, 08003 Barcelona, Spain, and Institut Català Nanotecnologia and
Institut Català d'Estudis i Recerca Avançada, Campus UAB Bellaterra,
Barcelona, Spain*

ABSTRACT

The local heat delivered by metallic nanoparticles selectively attached to their target can be used as a *molecular surgery* to safely remove toxic and clogging aggregates. We apply this principle to protein aggregates, in particular to the amyloid beta protein (Aβ) involved in Alzheimer's disease (AD), a neurodegenerative disease where unnaturally folded Aβ proteins self-assemble and deposit forming amyloid fibrils and plaques. We show the possibility to remotely redissolve these deposits and to interfere with their growth, using the local heat dissipated by gold nanoparticles (AuNP) selectively attached to the aggregates and irradiated with low gigahertz electromagnetic fields. Simultaneous tagging and manipulation by AuNP of Aβ at different stages of aggregation allow both, noninvasive exploration and dissolution of molecular aggregates.

Spontaneous self-assembly of molecular and nanoscale objects reflects information coded in the individual components, it is an essential part of nanotechnology, and it has a central role in life; for example, the components of a cell replicate and self-assemble into another cell during mitosis.[1]

Particular examples are proteins, which may experience conformational changes that results in an increment of the exposition of hydrophobic residues and, as a consequence, reduced solubility.[2] Afterward, these misfolded proteins self-assemble into insoluble fibrous deposits causing diseases called amyloidosis (Alzheimer's, Parkinson's, Huntington's, and type II diabetes among others).[3–6] In the process of self-

assembly, there is an equilibrium between soluble monomer and increasingly larger insoluble aggregates, *fibrils*, that entangle and precipitate,[7] forcing the equilibrium toward aggregated forms. Formation of these fibrils requires energy (for example, in the form of stirring), but once they are formed, they are stable. Vigorous shaking and sonication,[8] high hydrostatic pressure,[9] and temperature cycling[10] have the effect of reversing the natural equilibrium and redissolving the precipitates.

In this work we locally and remotely heat and dissolve amyloid deposits of Aβ_{1-42} (highly amyloidogenic[11]), a small protein involved in Alzheimer's disease, via the combined use of weak microwave fields and gold nanoparticles (AuNP), without any bulk heating. Irradiation as a means of remotely heating biological tissues mediated by inorganic nanoparticles has been extensively explored in a cellular scale as a cancer treatment,[12] and it was proposed to be useful at a molecular scale to dehybridize DNA without any bulk heating and without disturbing surrounding molecules.[13] In this case, the DNA responded as macroscopically heated at about 40 °C. It is worth noting that metallic nanoparticles

* Correspondence and requests for materials should be addressed to M.K. or V.P. (mkogan@ciq.uchile.cl, victor.puntes@icrea.es).
† Institut de Recerca Biomèdica de Barcelona, Parc Científic de Barcelona-UB.
‡ Departamento de Farmacología y Toxicología, Facultad de Ciencias Químicas, Universidad de Chile.
§ Departament de Física Fonamental, Universitat de Barcelona.
|| Departament de Química Orgànica, Universitat de Barcelona.
⊥ Centre Mediterrani d'Investigacions Marines i Ambientals, CMIMA-CSIC.
Institut Català Nanotecnologia and Institut Català d'Estudis i Recerca Avançada, Campus UAB Bellaterra.

are also useful for tagging and studying molecular structures,[14,15] together with predictions that nanotechnologies will have a deep impact in therapeutics.[16]

In detail, AuNPs were linked to the peptide H-Cys-Leu-Pro-Phe-Phe-AspNH$_2$ (Cys-PEP), which contains the sequence H-Leu-Pro-Phe-Phe-AspNH$_2$ (PEP) that selectively attaches to the Aβ aggregates,[17] forming the conjugated AuNP-Cys-PEP. It is believed that the peptides recognize a particular (hydrophobic) domain of the β-sheet structure (i.e., amino acids 17−20 of the hydrophobic core of Aβ);[17] however, fine structure of the Aβ fibrils is still unknown. An AuNP colloidal solution (10^{14} nanoparticles/ml) of about 10 nm in diameter, synthesized in the presence of sodium citrate, with uniform size distribution, was prepared. The gold precursor was injected into the refluxing citrate−water solution to narrow the size distribution.[18] We chose to use AuNP because of their nanometric size, biocompatibility, high electron density, and high (metallic) electron mobility. We used 10 nm particles because they are small enough to penetrate cell membranes, can survive harsh endosomal/lysosomal processes, and are able to carry targeting peptides.[19] AuNPs were incubated in the presence of Cys-PEP which was synthesized following a Fmoc strategy and solid-phase synthesis. The peptide sequence (PEP) selected in this study is a β-sheet breaker that in high ratio concentrations (PEP: Aβ) is able to block the amyloid fibril growth.[17] However, at such high concentrations, PEP only inhibits growth, to reverse growth, and push the equilibrium toward monomeric species, even higher concentrations of PEP should be used (1 equimolar to 20-fold molar excess with respect to Aβ), and it would be a slow process. The ratio of PEP:Aβ used in this study (1:10) is far too low to block fibril growth, as control experiments showed. The concentration of AuNP−Cys-PEP was 1 μM, and the relationship of AuNP−Cys-PEP:Aβ was 1:10. The conjugation of the AuNP with Cys-PEP shows a red shift in the surface plasmon resonance of the colloidal AuNP[20] (from 519 to 527 nm when Cys-PEP is attached to the AuNP). Agarose gel electrophoresis was used to isolate and detect conjugates[15] (see Supporting Information). We ran in parallel AuNP and AuNP−Cys-PEP; while the first was unable to migrate in the gel medium, AuNP−Cys-PEP migrated in a narrow band without any laddering showing the uniformity of the conjugates. This is correlated to the increased stability of AuNP−Cys-PEP solutions with respect to AuNP citrate-stabilized solutions, as recently shown by Levy et al.[21] X-ray photoelectron spectroscopy (XPS) analysis showed a fraction of the Au atoms (close to the fraction of surface atoms) bonded to S, indicating that AuNPs are fully coated with Cys-PEP, forming a monolayer on top of the particle surface (Supporting Information).

The conjugates were then incubated (at 37 °C) with a solution of A$\beta_{1−42}$ where fibrils spontaneously start growing and slowly form precipitates. Afterward, at different stages of growth, weak microwave fields (0.1 W) were applied. AuNP−Cys-PEP conjugates attached to the fibrils absorbed the radiation and dissipated energy causing disaggregation of the amyloid deposits and aggregates. Thus, when AuNP−
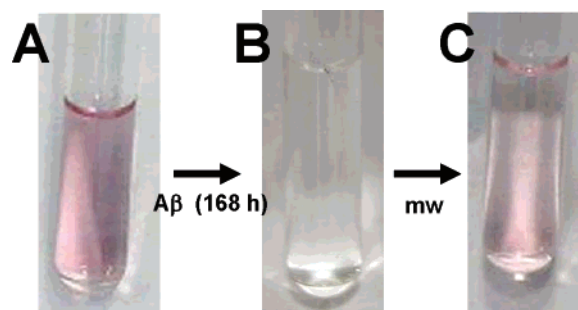

Figure 1. Remote dissolution of A$\beta_{1−42}$ precipitates. (A) AuNP−Cys-PEP solution mixed with A$\beta_{1−42}$ before the incubation. UV−vis absorption peak at 527 nm. (B) After incubation of AuNP−Cys-PEP with A$\beta_{1−42}$ for 7 days at 37 °C. No UV−vis absorption peak. (C) Irradiation of B for 8 h with 0.1 W and 12 GHz microwave field. UV−vis absorption peak at 527 nm.

Cys-PEP conjugates were incubated 7 days with A$\beta_{1−42}$, the initial red colored solution cleared off and a small black precipitate appeared. Irradiation of this solution dissolved the precipitates and brought back the original reddish color corresponding to dispersed AuNP−CysPEP (Figure 1).

The effects of mild microwaves fields on proteins influencing such as denaturation processes, conformational changes, and increased aggregation rates are known since microwave photons have the ability to interact with the ternary structures of proteins but not break chemical bonds.[22] We used a 12 GHz signal to avoid such resonances with protein modes since protein structures are not supposed to be affected by microwave frequencies greater than 8 GHz.[23] The power used, 100 mW, is 6 times smaller than that used by conventional mobile phones which usually work at 600 mW. In our control experiments the growth rate of the amyloid fibril was accelerated by the microwave field (Supporting Information). Likely microwaves increase the number of collisions between molecules and therefore the number of successful growth events. This is similar to the observed increase in deposit formation of albumin serum when microwaves where applied, all these cases without any bulk heating.[23] The power dissipated by one AuNP is $10^{−14}$ J/s, while the amyloid binding energy per bond is of $10^{−20}$ J.[24] Therefore, every microsecond the particle releases enough energy to break the fibril bond, while covalent bonds—up to 2 orders of magnitude stronger—are able to relax and are not broken (molecular vibrations are in the infrared range, MHz, i.e., microseconds). Besides, 8 h of irradiation would correspond to an increase of the particle temperature of about 100 K in a perfect adiabatic system. However, since in NPs the surface-to-volume ratio is very high, they dissipate energy rapidly, and after few minutes, the particle surface reaches a stationary temperature of the order of few microkelvins higher than that of the bulk[25] (Supporting Information).

To quantify the amount of fibrils in suspension, thioflavine T assays were performed in two types of sample: sample 1, large aggregates, after incubation of AuNP−Cys-PEP with Aβ for 7 days (Figure 2a) and sample 2, small aggregates, after incubation of the same for 16 h. At 7 days the Aβ is mainly precipitated (clear solution, see Figure 1b), while at 16 h the aggregation process is is at its early stage with the
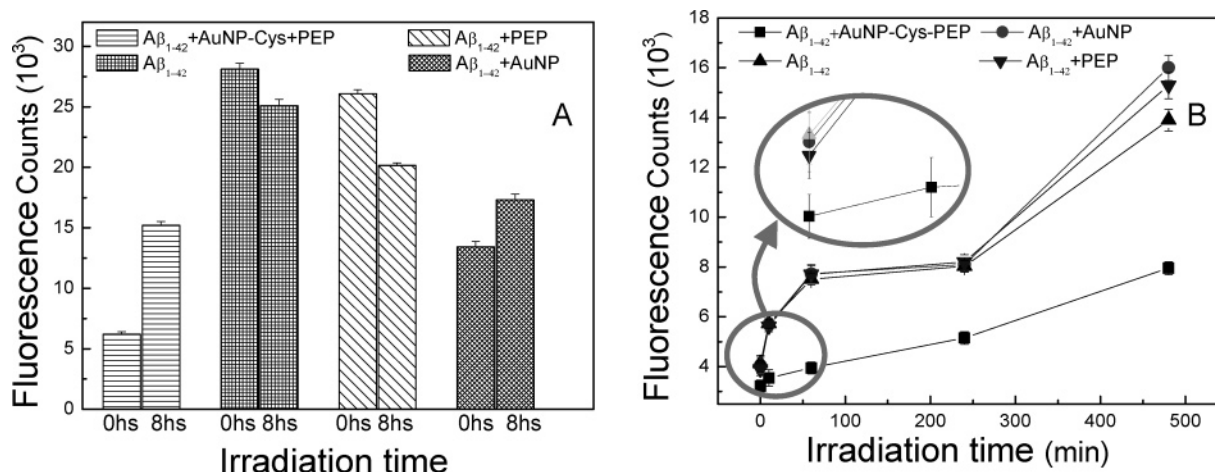
Figure 2. Variation of the intensity of thioflavine T fluorescence signal as a function of irradiation time. (A) For samples incubated during 7 days, after 8 h of irradiation, while the signal of samples without AuNP decreases, the sample with AuNP shows a modest increment in signal, and the sample with AuNP−Cys-PEP is almost triple its value. (B) Samples incubated during 16 h and irradiated for times up to 8 h. The measured signal in the sample is consistent with the coexistence of two competing mechanisms: the spontaneous fibril growth and the AuNP−Cys-PEP mediated cleavage of the fibril. The results are presented as mean ± standard deviation of at least four replica samples under each condition tested.

majority of species in solution. In this experiment the fluorescence signal is proportional to the amount of formed fibrils present in solution (nonprecipitated),[26] i.e., the baseline measurement of fibrils in solution. In the case of the $A\beta_{1-42}$ grown for 7 days (Figure 2a), when we irradiate the $A\beta_{1-42}$−AuNP−Cys-PEP precipitates, the fluorescence signal increases, which indicates that fibrils have passed from the precipitate to the solution. In control experiments without AuNP ($A\beta_{1-42}$ and $A\beta_{1-42}$ + PEP), the signal further decreased as precipitation evolved. The small increase of signal in control $A\beta_{1-42}$ + AuNP is likely due to nonspecific trapping of the AuNP by the precipitating amyloid fibrils. Regarding $A\beta$ alone, in Figure 2a the irradiation increases the agglomeration and deposition of $A\beta$ fibrils (and a consequent decrease of the thioflavine signal is observed). Thus, in samples of $A\beta$ alone incubated for 168 h that were not irradiated, no significant variation of the thioflavine signal was appreciated after 8 additional hours at room temperature under mild stirring (the time and conditions corresponding to the irradiation process).

We repeat the experiment with AuNP−Cys-PEP incubated with $A\beta_{1-42}$ for 16 h, to investigate how it interferes with the dynamics of protein deposit growth (Figure 2b). At these incubation times, fibrils are not mature yet, and their normal fate is further aggregation and thioflavine signal increase. Thus, when our sample is irradiated, we observe a steady growth of the fluorescence signal, indicating the growth of fibrils, up to a final value which is twice smaller than that in control experiments. The steady growth of the signal suggests both that AuNP−Cys-PEP, when released into the solution after irradiation, is able to attach itself again to the fibrils facilitating the fibrils being cut again or that the cut pieces are less amyloidogenic. Otherwise, after the first irradiation (and chopping) the fibrils would grow very fast due to the *nucleating* effect of the presence of small pieces (short oligomeric forms of $A\beta_{1-42}$ are very active and aggregate readily[8]). A fast signal increase observed at short

times in the control experiments is probably due to the onset of stirring and irradiation. In this case, irradiation of $A\beta$ alone increases its aggregation and the number of fibrils in solution (and a consequent increase of the thioflavine signal). Similarly, samples incubated for 16 h showed, after 8 additional hours at room temperature and mild stirring, a signal increase, smaller than that obtained when the sample was irradiated (Supporting Information).

We note that AuNPs do not get excited in the fluorimeter; however, they do absorb part of the radiation emitted by the fibers covered with thioflavine. When in solution, the concentration of AuNPs does not vary during the experiment and there is a constant−small−negative offset in the fluorimetry reading intensity which is evidenced in Figure 2b at $t = 0$. In addition, it seems, since concentrations are the same, that conjugated AuNPs quench more the thioflavine signal then free AuNP due to the particular spatial distribution. Besides, when the AuNPs are precipitated they do not absorb at the same frequencies anymore and this quenching effect disappears. In Figure 2a, discrepancies at time zero are also observed, which are also related to the larger incubation time and natural differences in the growth process or a chaperon effect limiting the growth rate which is induced by the steric effects of the large volume of the AuNP−Cys-PEP, as recently proposed in ref 27. Nevertheless, a smaller fluorescence is observed in all cases were AuNPs are present. These effects do not interfere with the observed evolution of aggregation−redissolution of the $A\beta$ aggregates.

To characterize the morphology of the aggregates before and after irradiation, we used transmission electron microscopy (TEM) (Figure 3 and Supporting Information). Before irradiation we observed amyloid fibrils profusely decorated with AuNP, presenting different AuNP densities depending on the relative concentrations of $A\beta_{1-42}$ versus AuNP−Cys-PEP and incubation times. There are virtually nonisolated AuNP−Cys-PEP, and it is rare to observe short fibrils or amorphous species. After irradiation, it is easy to qualitatively
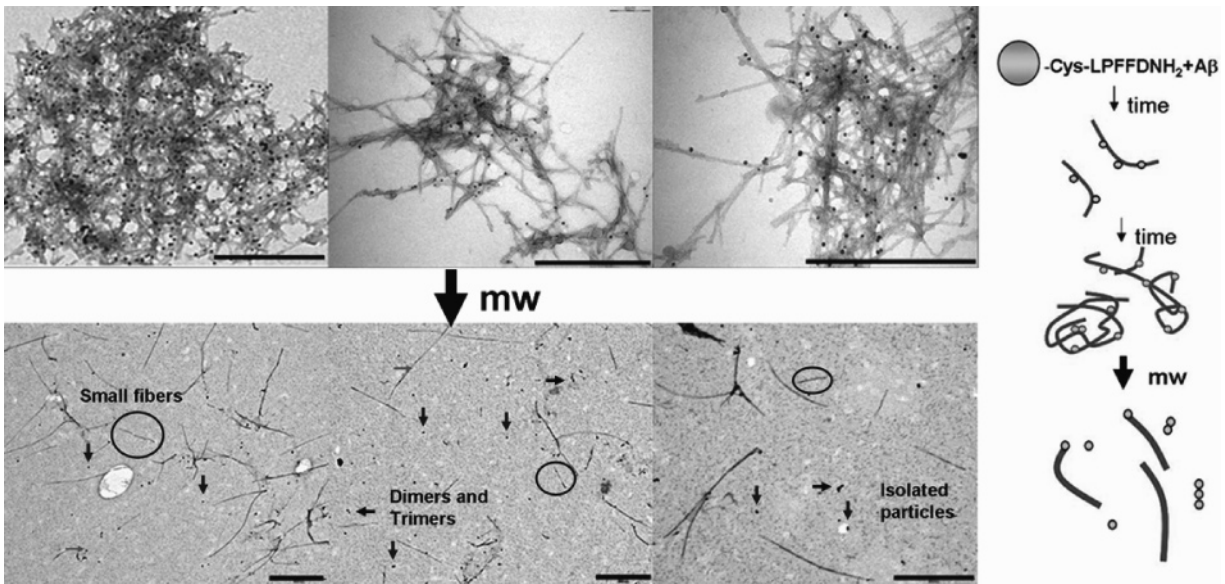
Figure 3. Electron microscopy of the solutions before and after irradiation. (top) Images of the AuNP−Cys-PEP bound to $A\beta_{1-42}$ aggregates after incubation of AuNP−Cys-PEP with 10 μM $A\beta_{1-42}$ for 48 h. (bottom) Images of the previous AuNP−Cys-PEP bound to $A\beta_{1-42}$ after 8 h of irradiation. Horizontal arrows indicate the presence of dimers and trimers, vertical arrows the presence of isolated particles, and circles the presence of small fibers. Bars are 500 nm.
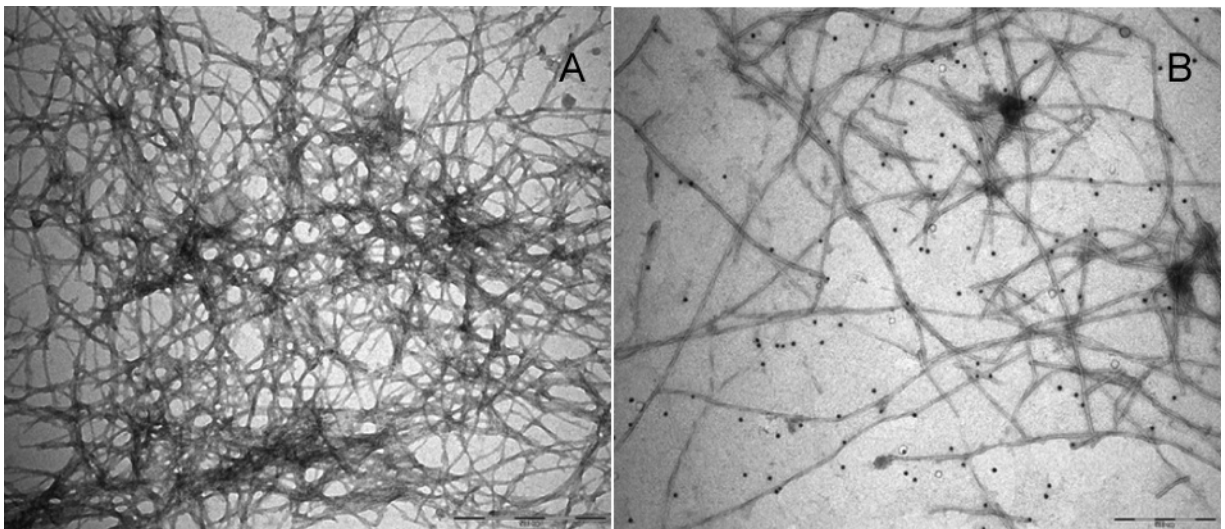

Figure 4. Electron microscopy of controls. (A) Control $A\beta_{1-42}$ alone incubated for 48 h and irradiated for 8 h (bar is 500 nm). AuNP−Cys-PEP + $A\beta_{1-42}$ grown for 48 h after 10 min of irradiation. (B) AuNP−Cys-PEP + $A\beta_{1-42}$ incubated for 48 h after 10 min of irradiation. Chopped fibrils and detached AuNP are already observable (bar is 200 nm).

observe the large impact of the local heating. In Figure 3, the diversity of AuNP and fibril species after irradiation is significantly larger.

In detail, small pieces of fibrils and amorphous aggregates appeared, AuNP agglomerates forming dimers and trimers also appeared, and the majority of AuNP−Cys-PEP (absorption peak still at 527 nm) was found detached from the fibrils. In addition, the remaining attached particles were found closer to the end of the fibrils than in the case of nonirradiated samples. Similar effects were observed at short times of irradiation (Figure 4b). Regarding dimers and trimers, as these structures have not been observed before or in controls, what brings the AuNP together must be a piece of the cut fibril. In control experiments using only AuNP−Cys-PEP, irradiated during 8 h, neither the detachment of the linker

(Cys-PEP) from the nanoparticle nor the agglomeration of AuNP−Cys-PEP were observed by TEM, surface plasmon resonance, or gel electrophoresis. The presence of abundant small pieces of fibrils after 8 h of irradiation also suggests that they are less active than before. In vivo experiments are being designed to test this hypothesis. The small and amorphous species in the background after irradiation suggests that when AuNP−Cys-PEP detaches from the fibril, water is allowed into the core of the fibril and the fibril shreds, as in ref 9. Besides TEM images of $A\beta$ alone irradiated or nonirradiated after 7 days of incubation showed large fibril agglomerates in both cases (Supporting Information). Therefore, in this case, thioflavine measurements were more descriptive than TEM images. In contrast, the irradiation effect mediated by the AuNP is easy to observe when
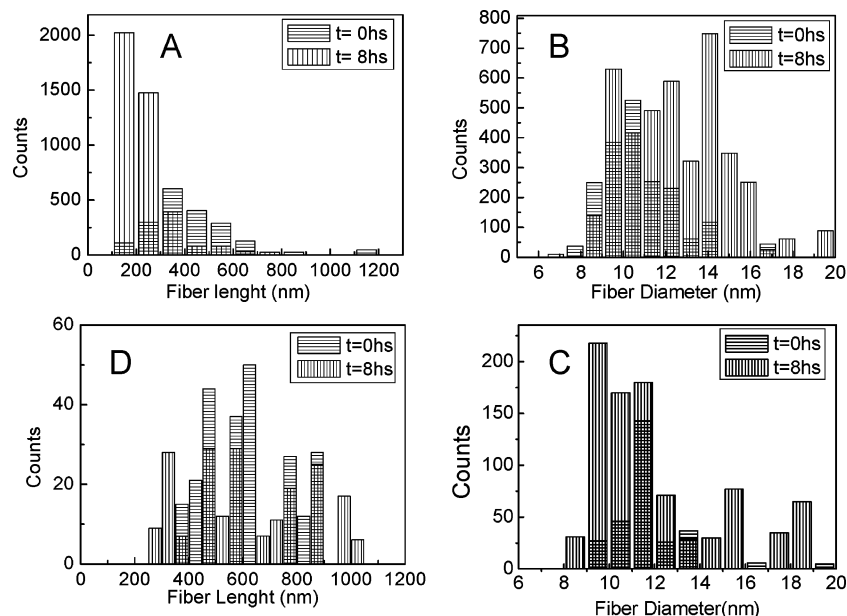
Figure 5. Image analysis of the TEM images. (A) Histogram of fibril length before and after 8 h of irradiation in samples Aβ_{1-42} + AuNP−Cys-PEP incubated for 48 h. Mean value before irradiation at 450 nm and after irradiation at 224 nm. (B) Histogram of fibril width before and after 8 h of irradiation in samples Aβ_{1-42} + AuNP−Cys-PEP incubated for 48 h. Mean value before irradiation at 11 nm and after irradiation at 13 nm. (C) Histogram of fibril length before and after 8 h of irradiation in samples Aβ_{1-42} incubated for 48 h. Mean value before irradiation at 600 nm and after irradiation at 615 nm. (D) Histogram of fibril width before and after 8 h of irradiation in samples Aβ_{1-42} incubated for 48 h. Mean value before irradiation at 11 nm and after irradiation at 11.5 nm. Experiments to extract images for analysis where repeated seven times.

comparing (i) samples of Aβ + AuNP−Cys-PEP incubated 48 h and irradiated 8 h (Figure 3 after irradiation) to (ii) Aβ alone incubated 48 h and irradiated 8 h (Figure 4a).

To extract additional information from the TEM, image processing was used to localize particles and fibrils by local thresholding using homemade software (Supporting Information). We have developed a program, written in C language, which implements all the required processing. The code allows statistical analysis on single images; after execution, the program returns the estimates of the number of fibrils contained in the given image and the averages of fibril diameter and fibril length. Multi-image processing can be obtained by jointly processing the individual results for the ensemble of images under consideration. Images are considered as graylevel pictures in which the graylevel is proportional to the intensity of the field recorded by the microscope. The first step of the process is to isolate a mask diferentiating fibrils from substrate and other structures. We have proceeded in a simple way to obtain this mask: we have just applied a simple threshold on the image graylevels. As fibrils appear as darker formations, for a given threshold value any pixel below this value is a priori considered to belong to a fibril, while the pixels with graylevels above the threshold are taken as nonfibril ones. Similar software to this was used in ref 28. Once the particles and the fibrils are mapped, thousands of events can be measured. To compare the size distribution of fibrils in the different experiments, since fibrils images are cut by the observing frame, we count the number of open-ends per fibril unit length. Assuming that each fibril has two ends, a clear decrease in the average fibril length is observed in these samples: from 450 nm after incubation (48 h at 37 °C) and

before irradiation to 224 nm after 8 h of irradiation. In both cases, long fibrils were found, up to 1125 nm before irradiation and 745 nm after (Figure 5a). In this count, features smaller than 100 nm were ignored. We also have observed a small variation of the average diameter of the fibril before (11 nm) and after (13 nm) irradiation; however, all the diameters appear around the same range (Figure 5b). This change in diameter is likely due to a modification in the Aβ fibril structure that leads to a progressive loss of its helical packing, as can be qualitatively observed in TEM images. Control experiments of Aβ alone before and after irradiation showed larger fibers in both cases and a nonsignificant variation of the fiber length, likely due to the fact that long fibers are cut by the observing TEM frame (before, 600 nm; after, 615 nm). Besides, fiber diameter stayed almost constant, showing a small increase, likely due to the loose helical packing due to agitation and, maybe, nonselective irradiation (before, 11 nm; after, 11.5 nm). In addition, in this experiment, the distribution of lengths between attached AuNP and fibril-ends shows also changes before and after irradiation. In the later case the distribution is shifted to lower values, i.e., AuNPs are closer to the end of the fibril, suggesting that AuNP−Cys-PEP has the ability to remain active and reattach itself to the remaining fibrils during the irradiation process (Supporting Information). Therefore, deactivation of the AuNP−Cys-PEP could be only related to the observed agglomerates of AuNP (dimers and trimers).

While TEM and thioflavine T assay give information about the morphology and the presence of formed fibrils in solution, filtration through a 0.22 μM filter followed by size exclusion chromatography (SEC) analysis shows an increment of low molecular weight species (monomer and

oligomers) which is in agreement with the conversion of high molecular weight aggregates to more soluble low molecular weight species during the irradiation. This increment was not observed in the control samples (Supporting Information).

All the observed effects on Aβ fibrils in the presence of the AuNP−Cys-PEP are *opposite* to macroscopic heating and microwave irradiation. When samples are macroscopically heated, an increase in temperature results in an increased aggregation rate. Similarly, weak microwaves fields are known to normally accelerate aggregation rates, probably by increasing the number of collision events that lead to binding,[22,23] as also observed in controls when Aβ fibrils alone are irradiated. Thus, attaching metallic AuNP to a target and applying microwave fields, allows a selective supply of energy to the system to manipulate molecular aggregation and deposits in a unique way.

Finally, the irradiated sample (Figure 1c) was left in the incubating chamber at 37 °C for 7 days to see if it went back to the precipitated state (Figure 1b). After these 7 days, no differences were observed in the tube or the surface plasmon resonance, thus indicating that the in vitro amyloidogenic potential has been significantly decreased.

Supporting Information Available: Additional details on the experimental procedures, nanoparticle conjugation,- TEM images, the image analysis, and size exclusion chromatography. This material is available free of charge via the Internet at http://pubs.acs.org.

References

(1) Whitesides, G. M.; Grzybowski, B. Self-Assembly at All Scales. *Science* **2002**, *295*, 2418−2421.

(2) Stefani, M.; Dobson, C. M. Protein aggregation and aggregate toxicity: new insights into protein folding, misfolding diseases and biological evolution *J. Mol. Med.* **2003**, *81*, 678−699.

(3) Small, D. H.; Mok, S. S.; Bornstein, J. C. Alzheimer's disease and Aβ toxicity: from top to bottom. *Nat. Rev. Neurosci.* **2001**, *2*, 595−598.

(4) DeMarco, M. L.; Daggett, V. From conversion to aggregation: protofibril formation of the prion protein. *Proc. Natl Acad. Sci. U.S.A.* **2004**, *101*, 2293−2298.

(5) Petkova, A. T.; Ishii, Y.; Balbach, J. J.; Antzutkin, O. N.; Leapman, R. D.; Delaglio, F.; Tycko, R. A structural model for Alzheimer's β-amyloid fibrils based on experimental constraints from solid-state NMR. *Proc. Natl Acad. Sci. U.S.A.* **2002**, *99*, 16742−16747.

(6) Arimon, M.; Diez-Perez, I.; Kogan, M. J.; Durany, N.; Giralt, E.; Sanz, F.; Fernandez-Busquets, X. Fine structure study of Abeta1-42 fibrillogenesis with atomic force microscopy *FASEB J.* **2005**, *19* (10), 1344-6.

(7) Harper, J. D.; Wong, S. S.; Lieber, C. M.; Lansbury, P. T. Assembly of amyloid protofibrils: an in vitro model for a possible early event in Alzheimer's disease. *Biochemistry* **1999**, *38*, 8972−8980.

(8) Serio, T. R.; Cashikar, A. G.; Kowal, A. S.; Sawicki, G. J.; Moslegi, J. J.; Serpell, L.; Arnsdorf, M. F.; Lindquist, S. L. Nucleated conformational conversion and the replication of conformational information by a prion determinant. *Science* **2000**, *289*, 1317−1321.

(9) Foguel, D.; Suarez, M. C.; Ferrão-Gonzales, A. D.; Porto, T. C. R.; Palmieri, L.; Einsiedler, C. M.; Andrade, L. R.; Lashuel, H. A.; Lansbury, P. T.; Kelly, J. W.; Silva, J. L. Dissociation of amyloid fibrils of α-synuclein and transthyretin by pressure reveals their reversible nature and the formation of water-excluded cavities. *Proc. Natl. Acad. Sci. U.S.A.* **2003**, *100*, 9831−9836.

(10) Gursky, O.; Aleshkov, S. Temperature-dependent beta-sheet formation in beta-amyloid Aβ(1−40) peptide in water: uncoupling beta-structure folding from aggregation. *Biochim. Biophys. Acta* **2000**, *1476*, 93−102.

(11) Citron, M.; Vigo-Pelfrey, C.; Teplow, D. B.; Miller, C.; Schenk, D.; Johnston, J.; Winblad, B.; Venizelos, N.; Lannfelt, L.; Selkoe, D. J. Amyloid β-protein and the genetics of Alzheimer's disease. *J. Biol. Chem.* **1996**, *271*, 18295−18298.

(12) Alexiou, C.; Arnold, W.; Klein, R. J.; Parak, F. G.; Hulin, P.; Bergemann, C.; Erhardt, W.; Wagenpfeil, S.; Lübbe, A. S. Locore-gional Cancer Treatment with Magnetic Drug Targeting. *Cancer Res.* **2000**, *60*, 6641−6648.

(13) Hamad-Schifferli, K.; Schwartz, J. J.; Santos, A. T.; Zhang, S.; Jacobson, J. M. Remote electronic control of DNA hybridization throughinductive coupling to an attached metal nanocrystal antenna. *Nature* **2002**, *415*, 152−155.

(14) Georganopoulou, D. G.; Chang, L.; Nam, J. M.; Thaxton, C. S.; Mufson, E. J.; Klein, W. L.; Mirkin, C. A. Nanoparticle-based detection in cerebral spinal fluid of a soluble pathogenic biomarker for Alzheimer's disease. *Proc. Natl. Acad. Sci. U.S.A.* **2005**, *102*, 2273−2276.

(15) Zanchet, D.; Michael, C. M.; Parak, W.; Gerion, D.; Alivisatos, A. P. Electrophoresis isolation of discrete Au Nanocrystal/DNA Conjugates. *Nano Lett.* **2001**, *1*, 32−35.

(16) LaVan, D. A.; Lynn, D. M.; Langer, R. Moving smaller in drug discovery and delivery *Nat. Rev. Drug Discovery* **2002**, *1*, 77−84.

(17) Soto, C.; Sigurdsson, E. M.; Morelli, L.; Kumar, R. A.; Castano, E. M.; Frangione, B. β-Sheet breaker peptides inhibit fibrillogenesis in a rat brain model of amyloidosis: implications for Alzheimer's therapy. *Nat. Med.* **1998**, *4*, 822−826.

(18) Puntes, V. F.; Zanchet, D.; Erdonmez, C.; Alivisatos, A. P. Synthesis of hcp-Co nanodisks. *J. Am. Chem. Soc.* **2002**, *124,* 12874−12880.

(19) Penn, S. G.; He, L.; Natan, M. J. Nanoparticles for bioanalysis. *Curr. Opin. Chem. Biol.* **2003**, *7*, 609−615.

(20) Storhoff, J. J.; Lazaorides, A. A.; Mucic, R. C.; Mirkin, C. A.; Letsinger, R. L.; Schatz, G. C. What controls the optical properties of DNA-Linked Gold Nanoparticle Assemblies. *J. Am. Chem. Soc.* **2000**, *122*, 4640−4650.

(21) Levy, R.; Thanh, N. T. K.; Doty, R. C.; Nichols, R. J.; Schiffrin, D. J.; Brust, M.; Fernig, D. G. Rational and combinatorial design of peptide capping ligands for Gold Nanoparticles. *J. Am. Chem. Soc.* **2004**, *126*, 10076−10084.

(22) Bohr, H.; Bohr, J. Microwave-enhanced folding and denaturation of globular proteins. *Phys. Rev. E* **2000**, *61*, 4310−4314.

(23) de Pomerai, D. I.; Smith, B.; Dawe, A.; North, K.; Smith, T.; Archer, D. B.; Duce, I. R.; Jones, D.; Peter, E.; Candido, M. Microwave radiation can alter protein conformation without bulk heating. *FEBS Lett.* **2003**, *543*, 93−97.

(24) Hammarstrom, P.; Wiseman, R. L.; Powers, E. T.; Kelly, J. W. Prevention of Transthryetin amyloid disease by changing protein misfolding energetics. *Science* **2003**, *299,* 713−716.

(25) Hergt, R.; Andrä, W.; d'Ambly, C. G.; Hilger, I.; Kaiser, W. A.; Richter, W.; Schmidt, H.-G. Physical Limits of Hyperthermia Using Magnetite Fine Particles *IEEE Trans. Magn.* **1998**, *34*, 3745−3754.

(26) LeVine, H. Thioflavine T interaction with synthetic Alzheimer's disease β-amyloid peptides: detection of amyloid aggregation in solution. *Protein Sci.* **1993**, *2*, 404−410.

(27) Gestwicki, J. E.; Crabtree, G. R.; Graef, I. A. Harnessing chaperones to generate small-molecule inhibitors of amyloid β Aggregation. *Science* **2004**, *306*, 865−869.

(28) Puntes, V. F.; Gorostiza, P.; Aruguete, D. M.; Bastus, N. G.; Alivisatos, A. P. Collective behavior in two-dimensional cobalt nanoparticle assemblies observed by magnetic force microscopy. *Nat. Mater.* **2004**, *3* 263−268.